# Bowl Meets Bowl. Electron Transfer in a Supramolecular Associate of a Fullerene Fragment

María Gallego, Joaquín Calbo, Juan Aragó, Rafael M. Krick Calderon, Fernando H. Liquido, Takahiro Iwamoto, Allison K. Greene, Edward A. Jackson, Emilio M. Pérez, Enrique Ortí, Dirk M. Guldi, Lawrence T. Scott, and Nazario Martín

# Bowl Meets Bowl. Electron Transfer in a Supramolecular Associate of a Fullerene Fragment

*María Gallego, Joaquín Calbo, Juan Aragó, Rafael M. Krick Calderon, Fernando H. Liquido, Takahiro Iwamoto, Allison K. Greene, Edward A. Jackson, Emilio M. Pérez, Enrique Ortí,* Dirk M. Guldi,* Lawrence T. Scott,* and Nazario Martín**

Abstract: Here, we investigate the association of a fullerene fragment, hemifullerene $C_{30}H_{12}$, by an electron donor bowl-shaped tetrathiafulvalene derivative (truxTTF). UV-vis titrations as well as DFT calculations support formation of the complex, for which an association constant of log Ka = 3.6 ± 0.3 in $CHCl_3$ at room temperature was calculated. Remarkably, electron transfer from truxTTF to $C_{30}H_{12}$ to form the fully charge-separated species takes place upon irradiation of the associate with light, constituting the first example in which a fullerene fragment mimicks the electron acceptor behaviour of the fullerenes within a supramolecular complex.

[*] M. Gallego, Prof. Dr. N. Martín
Departamento de Química Orgánica
Fac. C.C. Químicas, Universidad Complutense de Madrid
Av. Complutense s/n, E-28040 Madrid, Spain.
Fax: (+)34 913944103
E-mail: nazmar@quim.ucm.es
Homepage: www.ucm.es/info/fullerene/

J. Calbo, Dr. J. Aragó, Prof. Dr. E. Ortí
Instituto de Ciencia Molecular
Universidad de Valencia, E-46980 Paterna, Spain.
E-Mail: enrique.orti@uv.es

R. M. Krick-Calderon, Prof. Dr. D. M. Guldi
Department of Chemistry and Pharmacy & Interdisciplinary Center for Molecular Materials (ICMM)
Friedrich-Alexander-Universität Erlangen-Nürnberg
Egerlandstraße 3, D-91058 Erlangen, Germany.
E-mail: guldi@chemie.uni-erlangen.de.

F. H. Liquido, T. Iwamoto, A. K. Greene, E. A. Jackson, Prof. Dr. L. T. Scott
Merkert Chemistry Center, Boston College
Chestnut Hill, MA-02467-3860, USA.
E-mail: lawrence.scott@bc.edu

Dr. E. M. Pérez
IMDEA-nanociencia, C/ Faraday 9, Ciudad Universitaria de Cantoblanco, E-28049 Madrid, Spain.

[**] This work has been supported by the ERC (AdG Chirallcarbon ERC-2012-ADG_20120216), the MINECO of Spain (CTQ2011-24652, CTQ2011-25714, CTQ2012-31914, PIB2010JP-00196, and Consolider-Ingenio CSD2007-00010), the CAM (MADRISOLAR-2 S2009/PPQ-1533), the Generalitat Valenciana (PROMETEO/2012/053), and European FEDER funds (CTQ2012-31914). E.M.P. is thankful to the MINECO for a Ramón y Cajal research fellowship. M.G and J.C. acknowledge the Spanish Ministry of Education, Culture and Sport (MECD) for FPU grants.

The different nanoforms of carbon,[1] namely fullerenes,[2-3] carbon nanotubes,[4] and graphene,[5-8] each present distinct extraordinary properties that have attracted a great deal of attention in different areas of research. Fullerenes, and in particular $C_{60}$ and its derivatives, have been thoroughly studied as electron acceptors in fundamental investigations of photoinduced electron transfer (PET) processes, combined with a variety of electron donors in covalent and noncovalent dyads.[9-12] From an applied point of view, $C_{60}$ and $C_{70}$ derivatives are by far the most commonly utilized n-type semiconducting material in organic solar cells.[13-17] In the case of carbon nanotubes, both their mechanical and optoelectronic properties have been exploited to construct a variety of devices, including field-effect transistors and sensors.[18-22] Finally, graphene is currently considered to have potential to be the balm of Fierabras of carbon-based technologies. Transparent electrodes,[23-26] extremely sensitive sensors,[27-29] supercapacitors,[30-32] and light-weight high-performance materials[33] have all been postulated as potential applications of graphene.[34-35]

Molecular fragments of these carbon nanoforms[36] can serve as model systems for their investigation, with the added value of their synthetic availability in pure form with a well-defined molecular structure. The coordination of metal cations by fullerene fragments has been thoroughly studied, and they have also been used frequently to construct receptors for fullerenes,[37-39] but their binding by other organic hosts has not been so far investigated. Here, we present the first insights into the supramolecular association of a fullerene fragment (hemifullerene, $C_{30}H_{12}$) with a bowl-shaped electron donor molecule, based on a truxene core to which three dithiole rings are covalently attached (truxTTF).[40] The chemical structures of $C_{30}H_{12}$ and truxTTF are shown in Figure 1a.

Several syntheses[41-43] and two crystal structures[44] of hemifullerene $C_{30}H_{12}$ were reported a few years ago. In the solid state, two polymorphs were found, each of which showed a different packing motif, originating from the interaction between the $C_{30}H_{12}$ molecules. In the trigonal polymorph, bowl-in-bowl columnar stacks were found, an arrangement in which π–π interactions are maximized (Figure 1b). In the orthorhombic polymorph, each hemifullerene inserts one of its six-membered rings into the cavity of a neighbouring molecule, forming dimers in which both CH–π and π–π interactions play a primary role (Figure 1c). On the other hand, in truxTTF, a bowl-in-bowl arrangement is prevented by the protruding dithiole rings and, consequently, only the dimeric form in which one of the aromatic rings of each monomer is placed inside the cavity of the other is found (Figure 1d). Note that due to their

concave shape, both $C_{30}H_{12}$ and truxTTF are inherently chiral,[45] consequently, each is obtained as a racemic mixture of two enantiomers.

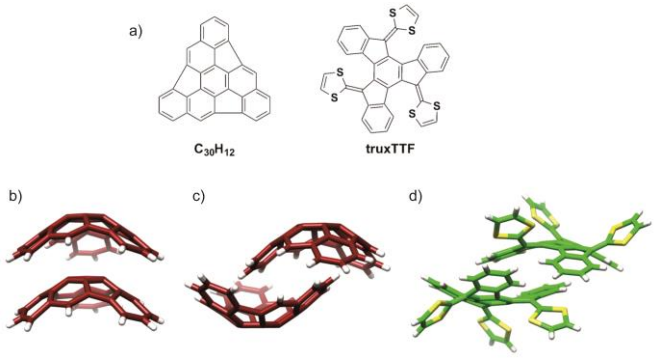


***Figure 1.*** a) Chemical structure of hemifullerene $C_{30}H_{12}$ and truxTTF. b) and c) Structures of the dimers formed by $C_{30}H_{12}$ (carbon atoms in dark red) in its trigonal and orthorhombic crystal polymorphs, respectively. d) Structure of the dimers formed by truxTTF (carbon atoms in green and sulfur in yellow) in its crystal packing.

Considering the ability of truxTTF to associate fullerenes,[40, 46] and its electron donor character, we reasoned that it should also be able to bind $C_{30}H_{12}$ forming heteromolecular bowl-bowl complexes. To explore this possibility, we first carried out density functional theory (DFT) calculations on four different supramolecular truxTTF•$C_{30}H_{12}$ models, which were rationally constructed from the crystallographic information on both $C_{30}H_{12}$ and truxTTF. All the models proposed were fully optimized using the revPBE0-D3 functional,[47-48] which is capable of capturing the dispersion effects and is one of the best density functionals to accurately describe supramolecular complexes governed by π–π interactions.[49] The revPBE0-D3 functional has been successfully applied in the structural and energetic characterization of related supramolecular nanoarchitectures between a tetrathiafulvalene derivative and a graphene sheet model.[50]

Figure 2 displays the minimum-energy structures (**1**–**4**) computed for the truxTTF•$C_{30}H_{12}$ heterodimer at the revPBE0-D3/cc-pVTZ level. The most relevant intermolecular distances in **1**–**4** are given in Figure S1 in the Supporting Information. The truxTTF•$C_{60}$ associate was also calculated at the same level of theory (Figure S2). In structures **1** and **2**, the convex surface of the $C_{30}H_{12}$ bowl perfectly matches the two concave cavities of the truxTTF host; i.e., either through the cavity formed by the carbon backbone (structure **1**) or through the cavity formed by the central benzene ring and the three dithiole rings (structure **2**). Both structures can be thus seen as bowl-in-bowl arrangements where π–π interactions are maximized. The concave cavities of truxTTF and $C_{30}H_{12}$ can also interact giving rise to heterodimers in which either a benzene or a dithiole ring of the truxTTF molecule is placed inside the concave cavity of the hemifullerene bowl (structures **3** and **4**, respectively). All the optimized heterodimeric structures **1**–**4** show close intermolecular contacts in the 2.5–3.7 Å range (see Figure S1), indicative of the positive noncovalent interaction between both bowls.

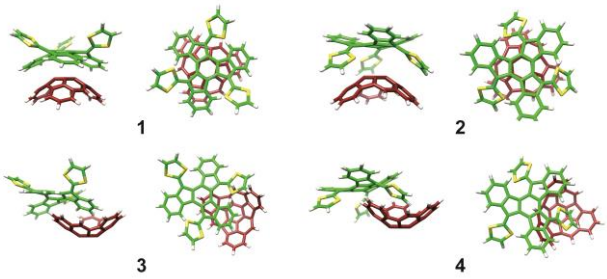


***Figure 2.*** Minimum-energy structures (**1**–**4**) computed for the truxTTF•$C_{30}H_{12}$ heterodimer at the revPBE0-D3/cc-pVTZ level. Carbon atoms of truxTTF are depicted in green, sulfur in yellow and hydrogen in white. Carbon atoms of $C_{30}H_{12}$ are depicted in red and hydrogen in white.

To assess the strength of the interaction between the truxTTF and $C_{30}H_{12}$ bowls, association energies for the previously optimized heterodimers were also calculated at revPBE0-D3/cc-pVTZ. The four supramolecular structures **1**–**4** exhibit significant gas-phase association energies, ranging from –21.0 and –19.4 kcal mol$^{-1}$ for **1** and **2**, respectively, to –25.2 and –28.5 kcal mol$^{-1}$ for **3** and **4**. The bowl-in-bowl arrangements are therefore significantly less stable than the staggered ones. The truxTTF•$C_{60}$ model system, for which we have experimentally calculated association constants in the range of log $K_a$ = 3–4 in a variety of solvents at room temperature,[40, 46] presents an association energy of –22.1 kcal mol$^{-1}$, which is very close to that computed for structure **1** due to the similarity in the concave-convex interaction.

The electronic properties of the truxTTF•$C_{30}H_{12}$ associate have also been theoretically investigated. Figure S3a sketches the highest occupied (HOMO–2 to HOMO) and lowest unoccupied (LUMO to LUMO+4) molecular orbitals computed at the revPBE0-D3/cc-pVTZ level for the most stable structure (**4**) of truxTTF•$C_{30}H_{12}$. Similar molecular orbital distributions are found for the rest of supramolecular structures **1**–**3** (Figure S3b). The HOMO, HOMO–1, and HOMO–2 spread over the electron-donor truxTTF moiety. In contrast, the LUMO, LUMO+1, and LUMO+2 are localized on the electron-acceptor $C_{30}H_{12}$ bowl, the LUMO+1 and LUMO+2 being almost degenerate. Above the LUMO+2, the LUMO+3 and LUMO+4 are again concentrated on the truxTTF bowl. The nature and energies calculated for the HOMOs and LUMOs of truxTTF•$C_{30}H_{12}$ therefore suggest that photoinduced charge-transfer processes from truxTTF to $C_{30}H_{12}$ should take place in the UV−Vis range.

Encouraged by the results of the theoretical calculations, we titrated truxTTF ($1.7 \times 10^{-4}$ M) with $C_{30}H_{12}$ ($0.8 \times 10^{-3}$ M) in $CHCl_3$ at room temperature. The electronic absorption spectra resulting from this titration experiment are depicted in Figure 3a. We observed a decrease in the intensity of the truxTTF absorption at λ = 450 nm, accompanied by the increase of a broad and a charge-transfer band in the 500–600 nm region. These spectral changes are analogous to those found in the titration of truxTTF vs $C_{60}$, albeit with a significantly less intense charge-transfer feature.[46] The results of three separate titration experiments were analysed utilizing Reactlab™ Equilibria software, affording a binding constant of log $K_a$ = 3.6 ± 0.3.

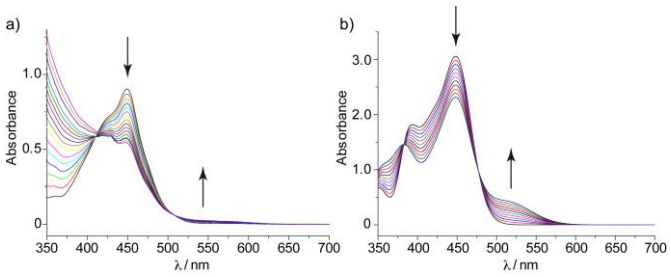


***Figure 3.*** a) Experimental UV−Vis spectra as obtained during the titration of truxTTF ($1.7 \times 10^{-4}$ M) with $C_{30}H_{12}$ ($0.8 \times 10^{-3}$ M) in $CHCl_3$ at room temperature. Each addition corresponds to 0.2 eq. b) TDDFT simulation of the absorption spectra of truxTTF as the ratio of truxTTF•$C_{30}H_{12}$ increases from 0 to 100% (B3LYP/cc-pVDZ calculations including $CHCl_3$ as solvent).

To gain more insight into the electronic nature of the absorption bands observed experimentally and their evolution during the titration experiment, the lowest-energy singlet excited states ($S_n$) of the truxTTF•$C_{30}H_{12}$ heterodimer and of isolated truxTTF were computed using the time-dependent DFT (TDDFT) approach and taking into account the solvent effects (see the Computational Details in the Supporting Information). Only the results obtained for the most stable structure (**4**) of truxTTF•$C_{30}H_{12}$ are discussed. TDDFT calculations predict the first two excited states $S_1$ and $S_2$ at 537 nm (2.31 eV) and 516 nm (2.40 eV) above the ground state $S_0$ with moderate oscillator strengths (*f*) of 0.036 and 0.046, respectively. The $S_0 \rightarrow S_1$ and $S_0 \rightarrow S_2$ electronic transitions are mainly described by one-electron promotions from the HOMO to the LUMO and LUMO+1, respectively. These transitions therefore imply a charge transfer from the electron-donor truxTTF, where the HOMO is located, to the electron-acceptor $C_{30}H_{12}$, where the LUMO and LUMO+1 spread (Figure S3a), and are the major contribution to the charge-transfer band experimentally recorded in the 500–600 nm range. Other charge-transfer transitions are computed around 500 nm but they are less intense (Table S1 in the Supporting Information). At higher energies, the $S_9$ (454 nm, 2.73 eV), $S_{10}$ (452 nm, 2.75 eV), and $S_{11}$ (445 nm, 2.78 eV) states are calculated very close in energy and present higher oscillator strengths (0.178, 0.178, and 0.093, respectively). The $S_0 \rightarrow S_9$, $S_0 \rightarrow S_{10}$, and $S_0 \rightarrow S_{11}$ electronic transitions mainly originate from the HOMO, HOMO–1 → LUMO+3, LUMO+4 one-electron excitations localized on truxTTF (Figure S3a), and give rise to the absorption band observed at 450 nm. It is to be noted that the oscillator strengths calculated for these transitions are significantly smaller than those computed for isolated truxTTF (0.277, 0.320, and 0.145, respectively).

A TDDFT simulation of the absorption spectra of the truxTTF chromophore, as the amount of truxTTF•$C_{30}H_{12}$ increases from 0 (spectrum of truxTTF) to 100%, is shown in Figure 3b. The simulation clearly reveals that the truxTTF band decreases in intensity as truxTTF•$C_{30}H_{12}$ is forming. This decrease is due to the smaller oscillator strengths computed for the truxTTF-centered transitions in the truxTTF•$C_{30}H_{12}$ complex. The charge-transfer band associated to the formation of truxTTF•$C_{30}H_{12}$ simultaneously increases in intensity. The theoretical simulation is in notable agreement with the experimental evolution of the absorption spectra and supports the formation of the supramolecular donor-acceptor truxTTF•$C_{30}H_{12}$ heterodimer.

Besides the ground state interactions, we turned to pump probe absorption measurements to unravel the processes following photoexcitation of truxTTF•$C_{30}H_{12}$ and their references, that is, truxTTF and $C_{30}H_{12}$. Immediately commencing with the 470 nm excitation of truxTTF, a new transient develops (Figure S4). Characteristics of the latter are a marked maximum in the visible at 530 nm and a broad, featureless transition that spans all throughout the near infrared. In addition, a marked ground-state bleaching is observed around 450 nm. It is of note that this excited state decays rapidly, as in other sulfur rich electron donors, with a lifetime of only 1.0 ± 0.1 ps. The short lifetime is rationalized by the presence of the sulfur atoms, with a strong second-order vibronic spin-orbit coupling, as it transforms into a much weaker absorbing state, for which a lifetime of 20 ± 1 ps is detected.

For $C_{30}H_{12}$, the singlet and triplet excited states upon 387 nm excitation include transient maxima at 515 and 586 nm, respectively (Figure S5). These reflect the singlet excited state that decays within 11 ns via intersystem crossing to the energetically low-lying triplet excited state.

Following 470 nm photoexcitation of truxTTF•$C_{30}H_{12}$ (1 to 5 ratio), the differential absorption changes are dominated by truxTTF-centered features (Figure 4). Within approximately 1.5 ± 0.5 ps, the latter give place, however, to a new transient with characteristics that include maxima at 440, 475, 495, 530 (sh), and 615 nm as well as a minimum at 450 nm. Notably, neither photoexcited $C_{30}H_{12}$ nor photoexcited truxTTF exhibit differential absorption changes that bear any significant resemblance (Figures S4 and S5). Thus, a tentative assignment of these features implies the formation of a charge-separated state.

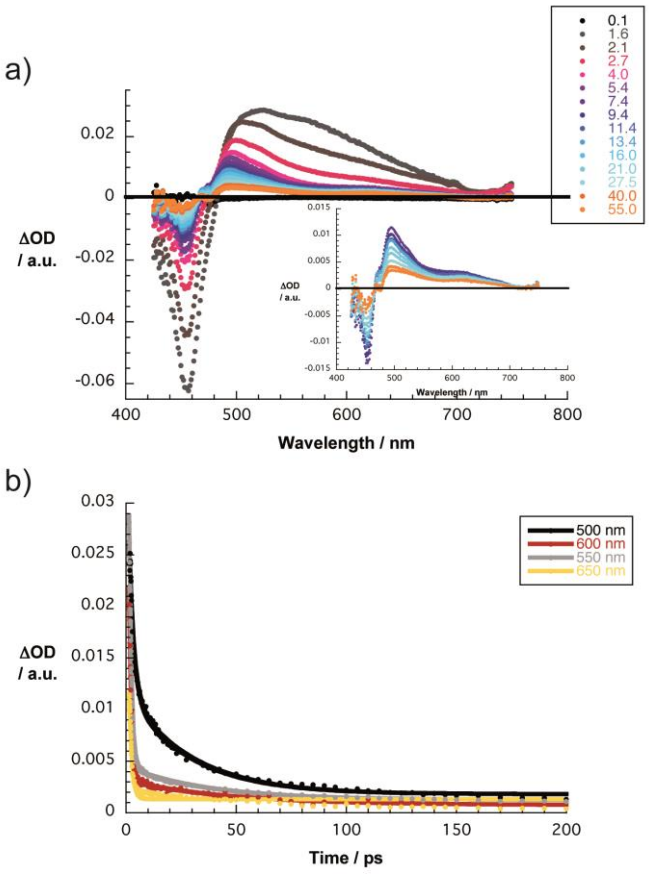


***Figure 4.*** a) Differential absorption spectra (visible) obtained upon femtosecond pump probe experiments (470 nm) of truxTTF•$C_{30}H_{12}$ (1:5 ratio) in chlorobenzene with time delays between 0.1 and 55.0 ps at room temperature. b) Time absorption profiles of the spectra shown above at 500 (black spectrum), 550 (grey spectrum), 600 (red

spectrum), and 650 nm (yellow spectrum) monitoring the charge transfer.

Support for this interpretation comes from spectroelectrochemical oxidation and reduction experiments with truxTTF and $C_{30}H_{12}$ in *ortho*-dichlorobenzene, respectively. For the former, upon applying a potential of +0.8 V versus Ag wire, maxima at 500 and 615 nm and a minimum at 450 nm are noted (Figure 5a). Importantly, resetting the potential back to 0 V led to a quantitative recovery of the starting spectrum. In the context of the latter, a potential of –1.0 V was chosen, and the differential absorption changes for the reduced $C_{30}H_{12}$ include maxima at 445, 475, 530, and 640 nm, which are accompanied by a 455 nm minimum (Figure 5b). Again, these changes were reversed upon resetting the applied potential back to 0 V. As such, the differential absorption changes upon photoexciting truxTTF•$C_{30}H_{12}$ (Figure 4) are in sound agreement with the superimposition of the spectroelectrochemically initiated oxidation and reduction of the truxTTF and hemifullerene, respectively. From multiwavelength analyses we derive rate constants of $6.6 \times 10^{11}$ and $1.0 \times 10^{10}$ $s^{-1}$ for the charge separation and charge recombination dynamics, respectively.

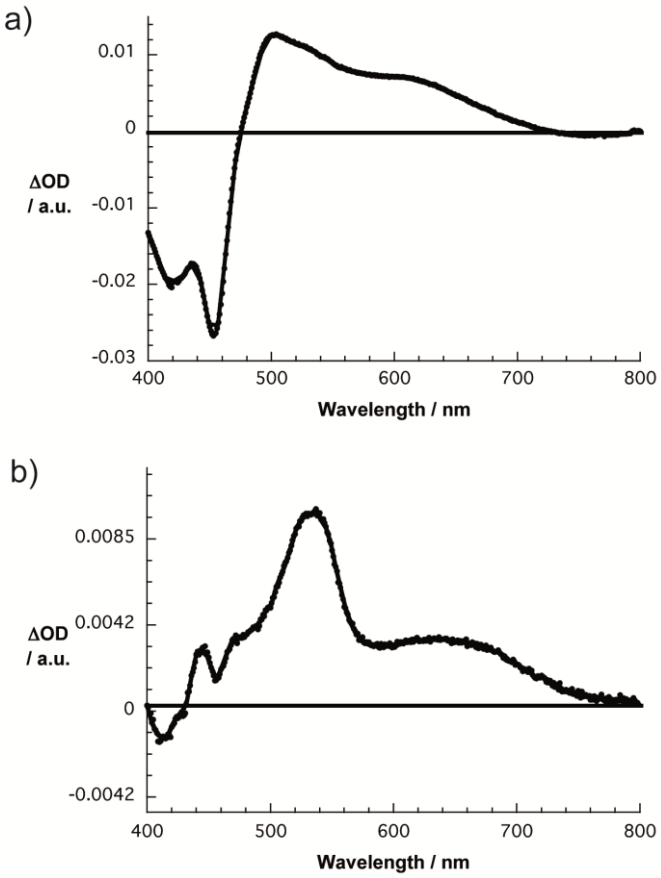


***Figure 5.*** Differential absorption spectra (visible) obtained upon spectroelectrochemical oxidation of truxTTF (a) and reduction of $C_{30}H_{12}$ (b) in deoxygenated *ortho*-dichlorobenzene containing 0.1 M $TBAPF_6$ with potentials versus Ag wire of +0.8 and –1.0 V, respectively.

To better understand the spectroelectrochemical data recorded for the truxTTF and $C_{30}H_{12}$ fragments, the theoretical UV–Vis spectra of the singly-oxidized truxTTF$^{\bullet+}$ and singly-reduced $C_{30}H_{12}^{\bullet-}$ species were computed. The spectra calculated for the neutral species were subtracted from the spectra of the oxidized/reduced systems to obtain a theoretical simulation of the differential absorption spectra (Figure 6). For the truxTTF fragment, the predicted spectrum (Figure 6a) is in excellent agreement with the experimental spectrum (Figure 5a). The long tail spreading from 550 to 800 nm originates from electron promotions from high-energy, doubly-occupied molecular orbitals to the single-occupied molecular orbital (SOMO) (doublet states $D_5$ to $D_9$). The peak observed at 500 nm is due to higher-energy excitations (states $D_{12}$ to $D_{15}$), where SOMO → LUMOs transitions are involved. The steep slope experimentally recorded at around 480 nm is nicely reproduced by the theoretical simulation and originates from the proximity in energy of the intense excitation to the doublet state $D_{17}$ in the cation and the excitation to the singlet state $S_2$ in the neutral species. The two-peak bleaching in the 400–450 nm region is due to the intense transitions ($S_5$-$S_6$ and $S_7$-$S_8$) of neutral truxTTF counterbalanced between them by the intense doublet excitation ($D_{24}$) in the cation. For the hemifullerene fragment, the theoretical simulation (Figure 6b) is in worse agreement with the experimental spectrum (Figure 5b) because the most intense band is calculated too high in energy. The lower-energy band appearing at 600–700 nm corresponds to doublet excitations ($D_3$-$D_5$) from the SOMO to higher-unoccupied molecular orbitals. The nearly-degeneracy of the LUMOs in neutral $C_{30}H_{12}$ is the origin of these low-energy transitions. Otherwise, the main features experimentally observed above 420 nm are assigned to doublet transitions ($D_8$ to $D_{20}$) implying electron excitations from doubly-occupied molecular orbitals to the SOMO.

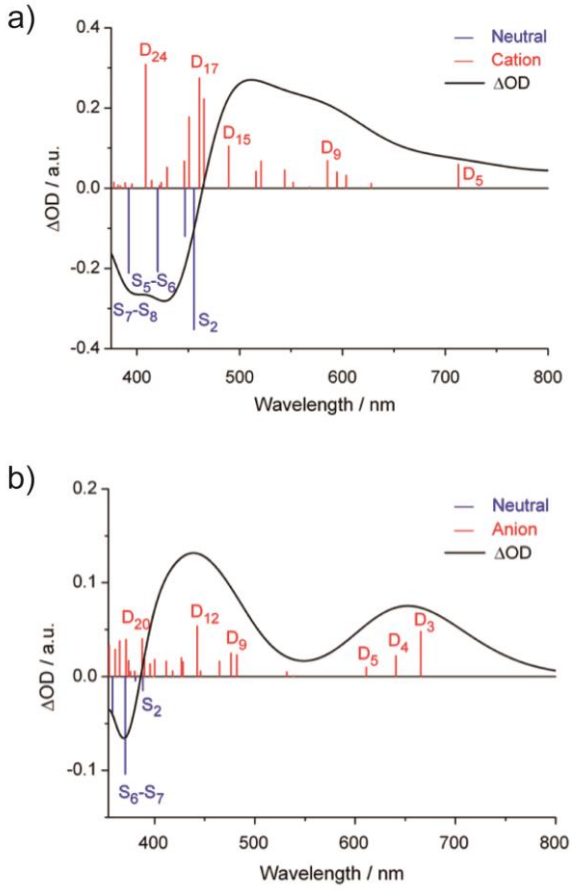


***Figure 6.*** TDDFT simulation of the differential absorption spectra calculated for truxTTF$^{\bullet+}$ (a) and $C_{30}H_{12}^{\bullet-}$ (b) at the B3LYP/cc-pVDZ level using *ortho*-dichlorobenzene as solvent.

In summary, we have corroborated the association of a fullerene fragment, namely hemifullerene $C_{30}H_{12}$, with a bowl-shaped electron donating truxTTF. The association was investigated experimentally through UV–Vis titrations. To this end, changes in the absorption spectra, most notably a decrease in the truxTTF absorption and formation of a weak charge transfer band, are clearly indicative for the truxTTF•$C_{30}H_{12}$ heterodimer in solution. Quantitatively, we calculated a binding constant of log $K_a$ = 3.6 ± 0.3 in $CHCl_3$ at room temperature, which is comparable to that found for the association of truxTTF with $C_{60}$. Calculations at the revPBE0-D3/cc-pVTZ level of theory supported the noncovalent interactions between truxTTF and $C_{30}H_{12}$; providing insight into the possible structure of the heterodimer and the nature of the changes observed during the UV–Vis titration.

Remarkably, femtosecond pump-probe experiments reveal the formation of a transient species that corresponds to a charge-separated truxTTF$^{\bullet+}$•$C_{30}H_{12}^{\bullet-}$ state. Overall, the latter assignment was backed by both spectroelectrochemical measurements and theoretical calculations. Analysis of the time evolution of these features afforded rate constants of 6.6 x $10^{11}$ and 1.0 x $10^{10}$ $s^{-1}$ for the charge separation and charge recombination dynamics, respectively. This is the first example of a fullerene fragment mimicking the charge transfer behavior of $C_{60}$, which paves the way to the study of other related fullerene fragments known so far, thus opening a new avenue for these electronically less-known carbon-based materials.

**Keywords:** density functional calculations · donor-acceptor systems · fullerenes · photoinduced electron transfer · supramolecular chemistry

[1] J. L. Delgado, M. A. Herranz, N. Martín, *J. Mater. Chem.* **2008**, *18*, 1417-1426.
[2] N. Martín, *Chem. Commun*. **2006**, 2093-2104.
[3] J. Delgado, S. Filippone, F. Giacalone, M. Herranz, B. Illescas, E. Pérez, N. Martín, *Top. Curr. Chem.* **2013**, 1-64.
[4] D. M. Guldi, N. Martín, Editors, *Carbon Nanotubes And Related Structures: Synthesis, Characterization, Functionalization, And Applications*, **2010**.
[5] M. J. Allen, V. C. Tung, R. B. Kaner, *Chem. Rev.* **2010**, *110*, 132-145.
[6] C. N. R. Rao, A. K. Sood, K. S. Subrahmanyam, A. Govindaraj, Angew. Chem. **2009**, *121*, 7890–7916; *Angew. Chem., Int. Ed.* **2009**, *48*, 7752-7777.
[7] A. K. Geim, *Science* **2009**, *324*, 1530-1534.
[8] A. K. Geim, K. S. Novoselov, *Nat. Mater.* **2007**, *6*, 183-191.
[9] N. Martín, L. Sánchez, M. A. Herranz, B. Illescas, D. M. Guldi, *Acc. Chem. Res.* **2007**, *40*, 1015-1024.
[10] D. Wróbel, A. Graja, *Coord. Chem. Rev.* **2011**, *255*, 2555-2577.
[11] S. Fukuzumi, T. Kojima, *J. Mater. Chem.* **2008**, *18*, 1427-1439.
[12] H. Imahori, *Org. Biomol. Chem.* **2004**, *2*, 1425-1433.
[13] G. Dennler, M. C. Scharber, C. J. Brabec, *Adv. Mater.* **2009**, *21*, 1323-1338.
[14] M. Helgesen, R. Søndergaard, F. C. Krebs, *J. Mater. Chem.* **2010**, *20*, 36-60.
[15] C. J. Brabec, S. Gowrisanker, J. J. M. Halls, D. Laird, S. Jia, S. P. Williams, *Adv. Mater.* **2010**, *22*, 3839-3856.
[16] H. Hoppe, N. S. Sariciftci, *J. Mater. Chem.* **2006**, *16*, 45-61.
[17] J. L. Delgado, P.-A. Bouit, S. Filippone, M. A. Herranz, N. Martín, *Chem. Commun*. **2010**, *46*, 4853–4865.
[18] J. M. Schnorr, T. M. Swager, *Chem. Mater.* **2011**, *23*, 646-657.
[19] C. Wang, K. Takei, T. Takahashi, A. Javey, *Chem. Soc. Rev.* **2013**, *42*, 2592-2609.
[20] S. Park, M. Vosguerichian, Z. Bao, *Nanoscale* **2013**, *5*, 1727-1752.
[21] S. N. Kim, J. F. Rusling, F. Papadimitrakopoulos, *Adv. Mater.* **2007**, *19*, 3214-3228.
[22] P. Avouris, J. Appenzeller, R. Martel, S. J. Wind, *Proc. of the IEEE* **2003**, *91*, 1772-1784.
[23] S. Bae, H. Kim, Y. Lee, X. Xu, J.-S. Park, Y. Zheng, J. Balakrishnan, T. Lei, H. R. Kim, Y. I. Song, Y.-J. Kim, K. S. Kim, B. Oezyilmaz, J.-H. Ahn, B. H. Hong, S. Iijima, *Nat. Nanotechnol.* **2010**, *5*, 574-578.
[24] X. Li, Y. Zhu, W. Cai, M. Borysiak, B. Han, D. Chen, R. D. Piner, L. Colombo, R. S. Ruoff, *Nano Lett.* **2009**, *9*, 4359-4363.
[25] K. S. Kim, Y. Zhao, H. Jang, S. Y. Lee, J. M. Kim, K. S. Kim, J.-H. Ahn, P. Kim, J.-Y. Choi, B. H. Hong, *Nature* **2009**, *457*, 706-710.
[26] X. Wang, L. Zhi, K. Müllen, *Nano Lett.* **2008**, *8*, 323-327.
[27] C.-H. Lu, H.-H. Yang, C.-L. Zhu, X. Chen, G.-N. Chen, Angew. Chem. **2009**, *121*, 4879–4881; *Angew. Chem., Int. Ed.* **2009**, *48*, 4785-4787.
[28] J. T. Robinson, F. K. Perkins, E. S. Snow, Z. Wei, P. E. Sheehan, *Nano Lett.* **2008**, *8*, 3137-3140.
[29] F. Schedin, A. K. Geim, S. V. Morozov, E. W. Hill, P. Blake, M. I. Katsnelson, K. S. Novoselov, *Nat. Mater.* **2007**, *6*, 652-655.
[30] Y. Zhu, S. Murali, M. D. Stoller, K. J. Ganesh, W. Cai, P. J. Ferreira, A. Pirkle, R. M. Wallace, K. A. Cychosz, M. Thommes, D. Su, E. A. Stach, R. S. Ruoff, *Science* **2011**, *332*, 1537-1541.
[31] K. Zhang, L. L. Zhang, X. S. Zhao, J. Wu, *Chem. Mater.* **2010**, *22*, 1392-1401.
[32] Y. Wang, Z. Shi, Y. Huang, Y. Ma, C. Wang, M. Chen, Y. Chen, *J. Phys. Chem. C* **2009**, *113*, 13103-13107.
[33] H. Hu, Z. Zhao, W. Wan, Y. Gogotsi, J. Qiu, *Adv. Mater.* **2013**, *25*, 2219-2223.
[34] X. Huang, Z. Yin, S. Wu, X. Qi, Q. He, Q. Zhang, Q. Yan, F. Boey, H. Zhang, *Small* **2011**, *7*, 1876-1902.
[35] A. K. Geim, A. H. MacDonald, *Physics Today* **2007**, *60*, 35-41.
[36] M. A. Petrukhina, L. T. Scott, John Wiley & Sons, **2012**, p. 413 pp.
[37] S. Mizyed, P. Georghiou, M. Bancu, B. Cuadra, A. K. Rai, P. Cheng, L. T. Scott, *J. Am. Chem. Soc.* **2001**, *123*, 12770-12774.
[38] P. E. Georghiou, A. H. Tran, S. Mizyed, M. Bancu, L. T. Scott, *J. Org. Chem.* **2005**, *70*, 6158-6163.
[39] L. N. Dawe, T. A. AlHujran, H.-A. Tran, J. I. Mercer, E. A. Jackson, L. T. Scott, P. E. Georghiou, *Chem. Commun.* **2012**, *48*, 5563-5565.
[40] E. M. Pérez, M. Sierra, L. Sánchez, M. R. Torres, R. Viruela, P. M. Viruela, E. Ortí, N. Martín, Angew. Chem. **2007**, *119*, 1879–1883; *Angew. Chem., Int. Ed.* **2007**, *46*, 1847-1851.
[41] G. Mehta, G. Panda, P. V. V. S. Sarma, *Tetrahedron Lett.* **1998**, *39*, 5835-5836.
[42] S. Hagen, M. S. Bratcher, M. S. Erickson, G. Zimmermann, L. T. Scott, Angew. Chem. **1997**, *109*, 407–409;*Angew. Chem., Int. Ed. Engl.* **1997**, *36*, 406-408.
[43] A. H. Abdourazak, Z. Marcinow, A. Sygula, R. Sygula, P. W. Rabideau, *J. Am. Chem. Soc.* **1995**, *117*, 6410-6411.
[44] M. A. Petrukhina, K. W. Andreini, L. Peng, L. T. Scott, Angew. Chem. **2004**, *116*, 5593–5597; *Angew. Chem., Int. Ed.* **2004**, *43*, 5477-5481.
[45] A. Dalla Cort, L. Mandolini, C. Pasquini, L. Schiaffino, *New J. Chem.* **2004**, *28*, 1198-1199.
[46] H. Isla, B. Grimm, E. M. Pérez, M. Rosario Torres, M. Angeles Herranz, R. Viruela, J. Ortí, E. Ortí, D. M. Guldi, N. Martín, *Chem. Sci.* **2012**, *3*, 498-508.
[47] Y. Zhang, W. Yang, *Phys. Rev. Lett.* **1998**, *80*, 890-890.
[48] S. Grimme, J. Antony, S. Ehrlich, H. Krieg, *J. Chem. Phys.* **2010**, *132*, 154104-154118.
[49] W. Hujo, S. Grimme, *J. Chem. Theory Comput.* **2011**, *7*, 3866-3871.
[50] F. G. Brunetti, H. Isla, J. Aragó, E. Ortí, E. M. Pérez, N. Martín, *Chem. Eur. J.* **2013**, *19*, 9843-9848.

**Entry for the Table of Contents** (Please choose one layout)

## *Fullerene fragments*

María Gallego, Joaquín Calbo, Juan Aragó, Rafael M. Krick Calderon, Fernando H. Liquido, Takahiro Iwamoto, Allison K. Greene, Edward A. Jackson, Emilio M. Pérez, Enrique Ortí,* Dirk M. Guldi,* Lawrence T. Scott,* and Nazario Martín* _____ **Page – Page**

Bowl Meets Bowl. Electron Transfer in a Supramolecular Associate of a Fullerene Fragment

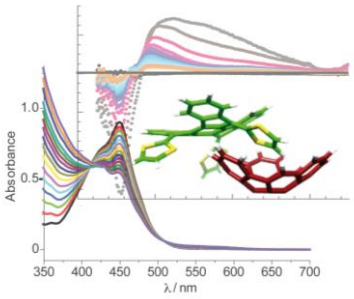


**Not a lonely bowl anymore.** We investigate the association of a fullerene fragment, hemifullerene $C_{30}H_{12}$, by an electron donor bowl-shaped tetrathiafulvalene derivative (truxTTF). Electron transfer from truxTTF to $C_{30}H_{12}$ to form the fully charge-separated species takes place upon irradiation of the associate with light, constituting the first example in which a fullerene fragment mimicks the electron acceptor behaviour of the fullerenes within a supramolecular complex.

# Supporting Information

**Bowl Meets Bowl. Electron Transfer in a Supramolecular Associate of a Fullerene Fragment.**

María Gallego,[1] Joaquín Calbo,[2] Juan Aragó,[2] Rafael M. Krick Calderon,[3] Fernando H. Liquido,[4] Takahiro Iwamoto,[4] Allison K. Greene,[4] Edward A. Jackson,[4] Emilio M. Pérez,[5] Enrique Ortí,[2,*] Dirk M. Guldi,[3,*] Lawrence T. Scott,[4,*] and Nazario Martín[1,5,*]

[1] Departamento de Química Orgánica, Fac. C.C. Químicas, Universidad Complutense de Madrid, Av. Complutense s/n, E-28040 Madrid, Spain. E-Mail: nazmar@quim.ucm.es

[2] Instituto de Ciencia Molecular, Universidad de Valencia, E-46980 Paterna, Spain. E-Mail: enrique.orti@uv.es

[3] Department of Chemistry and Pharmacy & Interdisciplinary Center for Molecular Materials (ICMM), Friedrich-Alexander-Universität Erlangen-Nürnberg, Egerlandstraße 3, D-91058 Erlangen, Germany. E-mail: guldi@chemie.uni-erlangen.de

[4] Merkert Chemistry Center, Boston College, Chestnut Hill, MA-02467-3860, USA. E-mail: lawrence.scott@bc.edu

[5] IMDEA-nanociencia, C/ Faraday 9, Ciudad Universitaria de Cantoblanco, E-28049 Madrid, Spain.

## Computational Details

Geometry optimizations of the supramolecular truxTTF•$C_{30}H_{12}$ heterodimers **1**–**4** were performed within the density functional theory (DFT) framework using the revPBE0 correlation-exchange functional in combination with the Grimme dispersion correction -D3 (revPBE0-D3).[1,2] Note that the original damping function in the -D3 approach has been replaced by the Becke-Johnson damping function to provide a better performance.[3] The choice of the exchange-correlation functional revPBE0 is justified by its excellent performance when studying the very popular S22[4] and S66[5] non-covalent interaction databases[6] as well as when applied to other related supramolecular systems.[7-10] The correlation-consistent cc-pVTZ basis set was applied throughtout.[11] The "resolution of identity" (RI)[12] and "chain of spheres" (COSX)[13] techniques, for the Coulomb and exchange integrals, respectively, were used to alleviate the computational cost of the more demanding steps.

On the previously optimized structures (both for the heterodimer and for the isolated moieties), single-energy calculations at the revPBE0-D3/cc-pVTZ level were performed to compute the association binding energies. Note that the three-body contribution to the dispersion energy has been included because it can be significant for medium and large supramolecular systems.[14] The association energy in each heterodimer was computed as the difference between the energy of the associate and the sum of the energies for the two constituting fragments [$\Delta E_{assoc} = E$(heterodimer) – $E$(truxTTF) – $E$($C_{30}H_{12}$ or $C_{60}$)]. Geometry optimizations and single-point energy calculations at the revPBE0-D3/cc-pVTZ level were performed using the ORCA program package (version 2.9.0).[15] Molecular orbitals were plotted using the Chemcraft 1.6 software with electron density contours of 0.03 e bohr$^{-3}$.[16]

Vertical electronic transition energies for the ground-state optimized geometries of structures **1**–**4** were computed in the framework of the time-dependent density functional theory (TDDFT)[17] using the Gaussian 09 (revision D.01)[18] suite of programs. The lowest 40 singlet excited states of the truxTTF•$C_{30}H_{12}$ heterodimer and its individual fragments were computed at the B3LYP/cc-pVDZ level of theory. Solvent effects were taken into account by means of the polarizable continuum model (PCM) using chloroform ($CHCl_3$) as a solvent.[19,20] The TDDFT simulation displayed in the main text (Figure 4b) corresponds to the absorption spectra of truxTTF as the ratio of truxTTF•$C_{30}H_{12}$ increases from 0 (pure truxTTF) to 100% (all the truxTTF is complexed as truxTTF•$C_{30}H_{12}$) in steps of 10%. The sigma parameter used for the Gaussian functions in the convolution of the spectra was set to 0.15 eV. During the titration experiment, there is an increasing amount of $C_{30}H_{12}$ that is not associated to truxTTF and contributes to the experimental absorption spectrum with the growth of an intense band below 350 nm where the characteristic intense peak of $C_{30}H_{12}$ is found. The theoretical simulation does not consider the electronic transitions of isolated $C_{30}H_{12}$ involved in this band because they are not relevant for the characterization of the supramolecular truxTTF•$C_{30}H_{12}$ complex.

The truxTTF and hemifullerene fragments in its cation and anion state, respectively, were also computed in order to understand the spectroelectrochemical oxidation and reduction experiments carried out in *ortho*-dichlorobenzene. The $truxTTF^{+}$ and $C_{30}H_{12}^{-}$ species were fully optimized at the rev-PBE0-D3/cc-pVTZ level taking into account solvent effects using PCM and *ortho*-dichlorobenzene as solvent. Their neutral counterparts were also optimized at the same level of theory. The TDDFT simulation of the differential absorption spectra for $truxTTF^{+}$ and $C_{30}H_{12}^{-}$ (Figure 6 in the main text) was obtained by subtracting the spectrum of the neutral form of each fragment to the calculated spectrum of the cation and anion, respectively. TDDFT calculations were performed at the B3LYP/cc-pVDZ level using *ortho*-dichlorobenzene as solvent.

References:


(1) Zhang, Y.; Yang, W. *Phys. Rev. Lett.* **1998**, *80*, 890.
(2) Grimme, S.; Antony, J.; Ehrlich, S.; Krieg, H. *J. Chem. Phys.* **2010**, *132*, 154104.
(3) Grimme, S.; Ehrlich, S.; Goerigk, L. *J. Comput. Chem.* **2011**, *32*, 1456.
(4) Jurecka, P.; Sponer, J.; Cerny, J.; Hobza, P. *PCCP* **2006**, *8*, 1985.
(5) Řezáč, J.; Riley, K. E.; Hobza, P. *J. Chem. Theory Comput.* **2011**, *7*, 2427.
(6) Hujo, W.; Grimme, S. *J. Chem. Theory Comput.* **2011**, *7*, 3866.
(7) Grimme, S.; Hujo, W.; Kirchner, B. *Phys. Chem. Chem. Phys.* **2012**, *14*, 4875.
(8) Rana, M. K.; Koh, H. S.; Hwang, J.; Siegel, D. J. *J. Phys. Chem. C* **2012**, *116*, 16957.
(9) Tkatchenko, A.; von Lilienfeld, O. A. *Phys. Rev. B* **2008**, *78*, 045116.
(10) Goltl, F.; Hafner, J. *J. Chem. Phys.* **2011**, *134*, 064102.
(11) Dunning, J. T. H. *J. Chem. Phys.* **1989**, *90*, 1007.
(12) Eichkorn, K.; Treutler, O.; Öhm, H.; Häser, M.; Ahlrichs, R. *Chem. Phys. Lett.* **1995**, *240*, 283.
(13) Neese, F.; Wennmohs, F.; Hansen, A.; Becker, U. *Chem. Phys.* **2009**, *356*, 98.
(14) Grimme, S. *Chem. Eur. J.* **2012**, *18*, 9955.
(15) Neese, F. *WIREs Comput. Mol. Sci.* **2012**, *2*, 73.
(16) http://www.chemcraftprog.com
(17) Casida, M. E.; Jamorski, C.; Casida, K. C.; Salahub, D. R. *J. Chem. Phys.* **1998**, *108*, 4439.
(18) Gaussian 09, Revision D.01, Frisch, M. J.; Trucks, G. W.; Schlegel, H. B.; Scuseria, G. E.; Robb, M. A.; Cheeseman, J. R.; Scalmani, G.; Barone, V.; Mennucci, B.; Petersson, G. A.; Nakatsuji, H.; Caricato, M.; Li, X.; Hratchian, H. P.; Izmaylov, A. F.; Bloino, J.; Zheng, G.; Sonnenberg, J. L.; Hada, M.; Ehara, M.; Toyota, K.; Fukuda, R.; Hasegawa, J.; Ishida, M.; Nakajima, T.; Honda, Y.; Kitao, O.; Nakai, H.; Vreven, T.; Montgomery, J. A.; Peralta, J. E.; Ogliaro, F.; Bearpark, M.; Heyd, J. J.; Brothers, E.; Kudin, K. N.; Staroverov, V. N.; Kobayashi, R.; Normand, J.; Raghavachari, K.; Rendell, A.; Burant, J. C.; Iyengar, S. S.; Tomasi, J.; Cossi, M.; Rega, N.; Millam, J. M.; Klene, M.; Knox, J. E.; Cross, J. B.; Bakken, V.; Adamo, C.; Jaramillo, J.; Gomperts, R.; Stratmann, R. E.; Yazyev, O.; Austin, A. J.; Cammi, R.; Pomelli, C.; Ochterski, J. W.; Martin, R. L.; Morokuma, K.; Zakrzewski, V. G.; Voth, G. A.; Salvador, P.; Dannenberg, J. J.; Dapprich, S.; Daniels, A. D.; Farkas; Foresman, J. B.; Ortiz, J. V.; Cioslowski, J.; Fox, D. J., Gaussian, Inc., Wallingford CT, **2009**.
(19) Tomasi, J.; Persico, M. *Chem. Rev.* **1994**, *94*, 2027.
(20) Cramer, C. S.; Thrular, D. G. *Solvent Effects and Chemical Reactivity*; Kluwer: Dordrecht, 1996.

Structure **1**

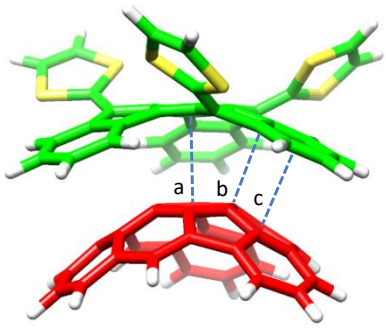


| Distance | revPBE0-D3/cc-pVTZ (Å) |
|---|---|
| a | 3.26 |
| b | 3.08 |
| c | 3.28 |

Structure **2**

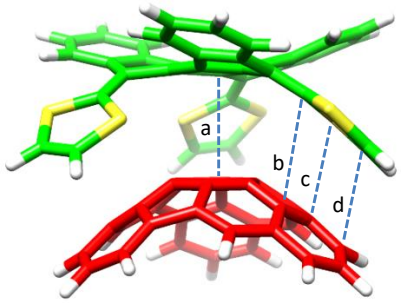


| Distance | revPBE0-D3/cc-pVTZ (Å) |
|---|---|
| a | 3.71 |
| b | 3.66 |
| c | 3.37 |
| d | 3.49 |

Structure **3**

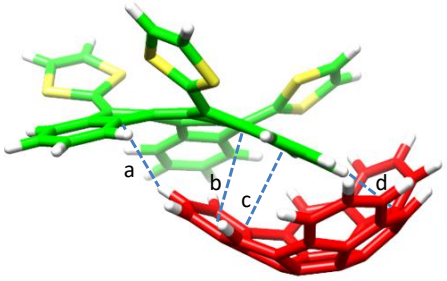


| Distance | revPBE0-D3/cc-pVTZ (Å) |
|---|---|
| a | 2.73 |
| b | 3.65 |
| c | 3.54 |
| d | 2.56 |

Structure **4**

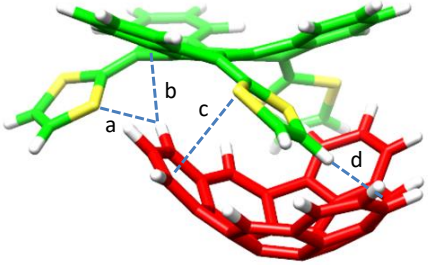


| Distance | revPBE0-D3/cc-pVTZ (Å) |
|---|---|
| a | 2.76 |
| b | 2.69 |
| c | 3.62 |
| d | 2.52 |

**Figure S1.** Selected intermolecular distances computed for structures **1**–**4** at the revPBE0-D3/cc-pVTZ level.

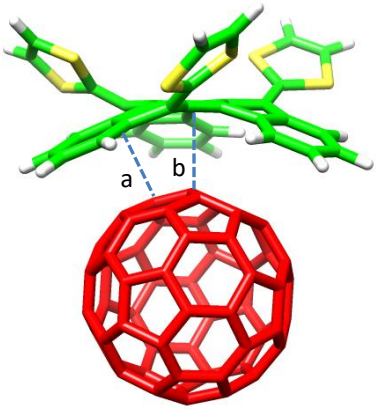


| Distance | revPBE0-D3/cc-pVTZ (Å) |
|---|---|
| a | 3.27 |
| b | 3.07 |

**Figure S2.** Selected intermolecular distances computed for the truxTTF•$C_{60}$ associate at the revPBE0-D3/cc-pVTZ level.

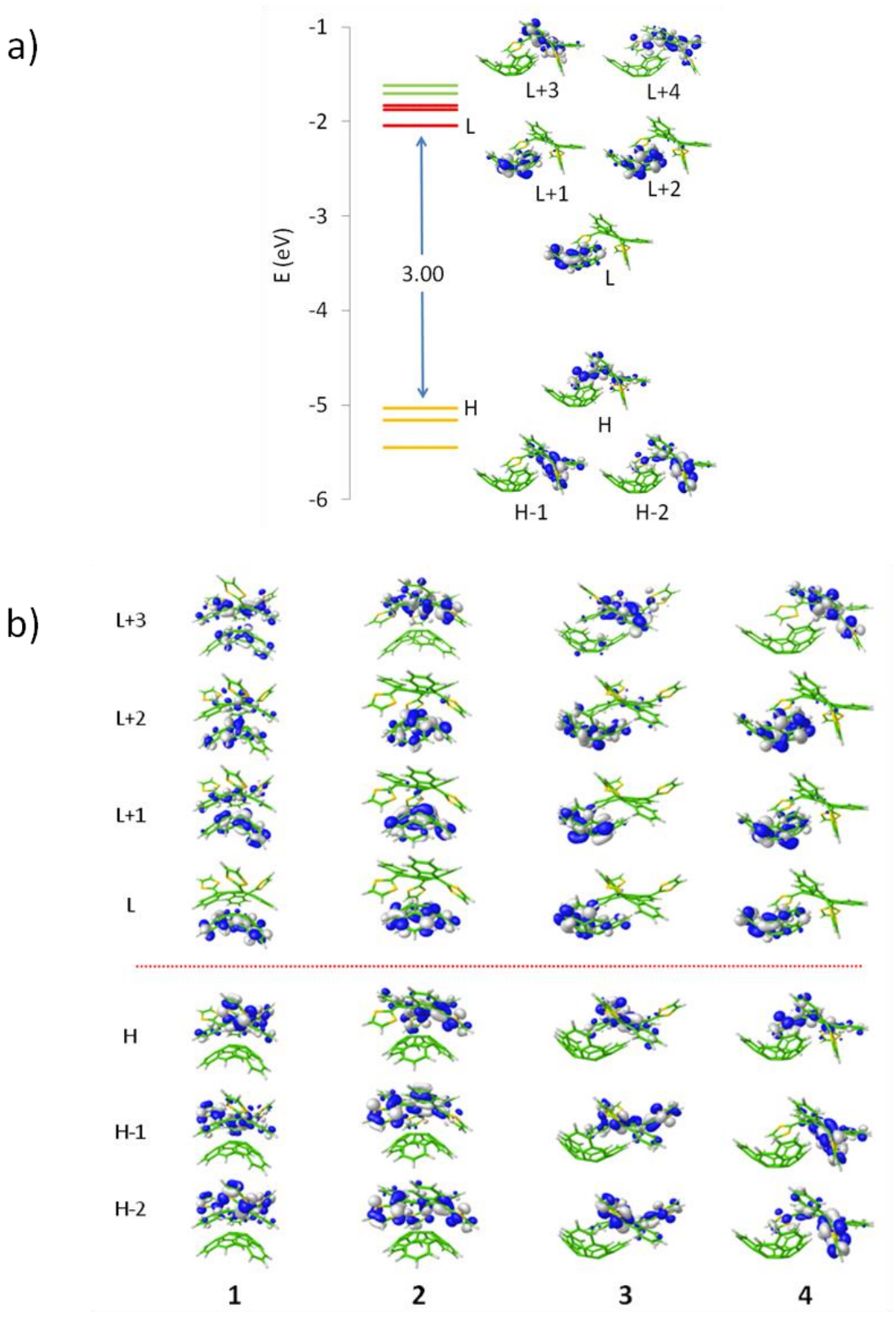


**Figure S3.** a) Electron density contours (0.03 e bohr$^{-3}$) and energies calculated for the HOMOs and LUMOs of structure **4** at the revPBE0-D3/cc-pVTZ level. H and L denote HOMO and LUMO, respectively. b) Electron density contours (0.03 e bohr$^{-3}$) computed for structures **1**–**4** at the revPBE0-D3/cc-pVTZ level.

**Table S1.** Lowest singlet excited states calculated at the TDDFT level (B3LYP/cc-pVDZ in $CHCl_3$) for structure **4** of the truxTTF•$C_{30}H_{12}$ heterodimer. Vertical excitation energies (*E*), oscillator strengths (*f*), dominant monoexcitations with contributions (within parentheses) greater than 15%, and description of the excited states are given.

| State | *E* (eV) | *E* (nm) | *f* | Monoexcitations[a] | | Description[b] |
|---|---|---|---|---|---|---|
| $S_1$ | 2.31 | 537 | 0.0355 | H → L | (83) | CT |
| $S_2$ | 2.40 | 516 | 0.0464 | H → L+1 | (76) | CT |
| $S_3$ | 2.43 | 510 | 0.0054 | H → L+2 | (82) | CT |
| $S_4$ | 2.48 | 500 | 0.0183 | H–1 → L | (55) | CT |
| | | | | H–1 → L+2 | (19) | CT |
| $S_5$ | 2.52 | 493 | 0.0182 | H → L+3 | (52) | truxTTF |
| | | | | H–1 → L | (21) | CT |
| $S_6$ | 2.58 | 480 | 0.0271 | H–1 → L+1 | (73) | CT |
| $S_7$ | 2.61 | 476 | 0.0096 | H–1 → L+2 | (74) | CT |
| $S_8$ | 2.72 | 456 | 0.0516 | H–2 → L | (41) | CT |
| | | | | H–1 → L+3 | (15) | truxTTF |
| $S_9$ | 2.73 | 454 | 0.1776 | H–1 → L+3 | (47) | truxTTF |
| | | | | H–2 → L | (21) | CT |
| $S_{10}$ | 2.75 | 452 | 0.1776 | H → L+4 | (46) | truxTTF |
| | | | | H–1 → L+4 | (26) | truxTTF |
| $S_{11}$ | 2.78 | 445 | 0.0929 | H–1 → L+4 | (37) | truxTTF |
| | | | | H → L+4 | (34) | truxTTF |
| | | | | H–1 → L+3 | (20) | truxTTF |
| $S_{12}$ | 2.82 | 440 | 0.0317 | H–2 → L+1 | (71) | CT |

[a]H and L donote HOMO and LUMO, respectively. The atomic orbital composition of the MOs coincides with that sketched in Figure S3a for structure **4**. [b]CT and truxTTF denote charge-transfer and truxTTF-centered electronic transitions, respectively.

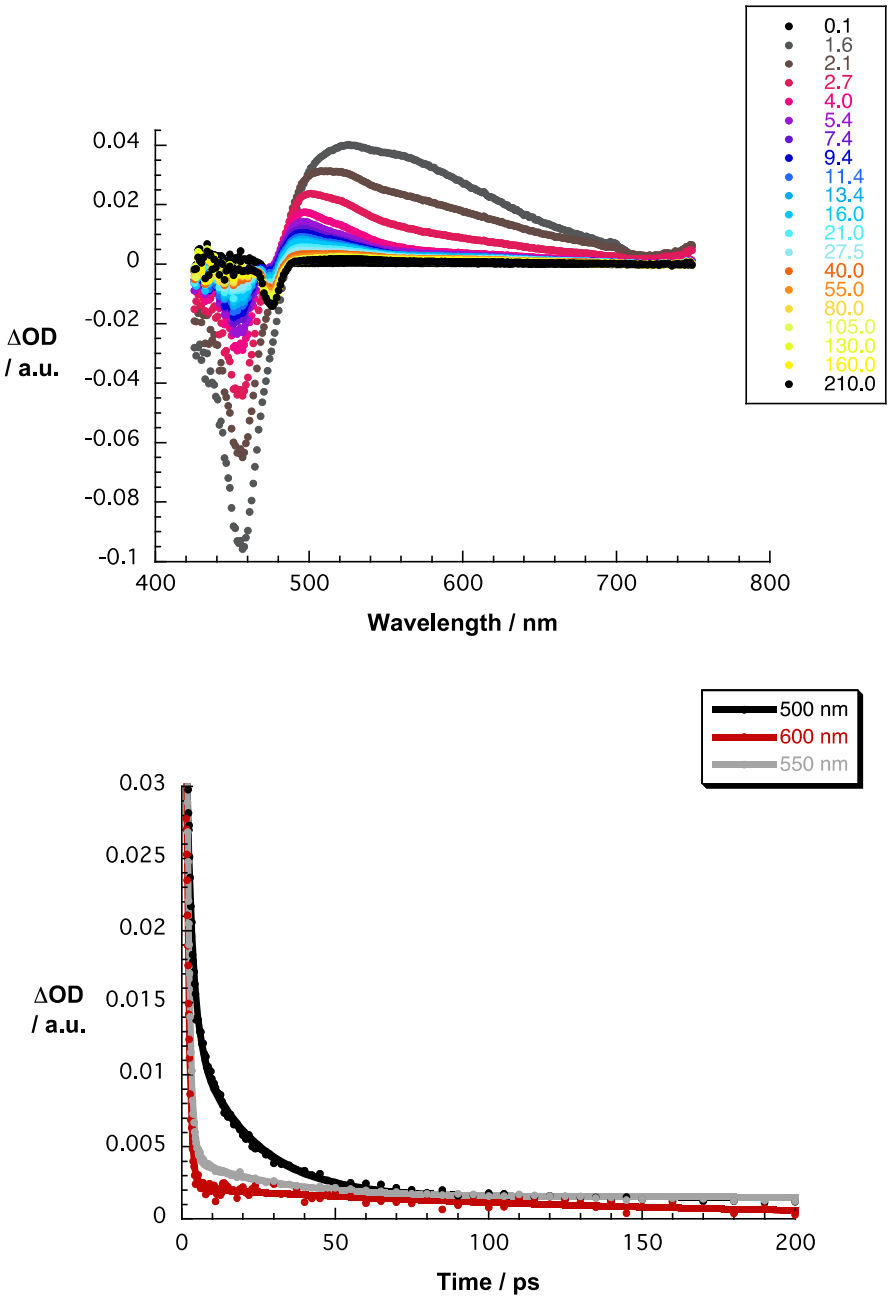


**Figure S4**: Top: differential absorption spectra (visible) obtained upon femtosecond pump probe experiments (470 nm) of truxene in chlorobenzene with time delays between 0.1 and 210.0 ps at room temperature. Bottom: time absorption profiles of the spectra shown above at 500 (black spectrum), 550 (grey spectrum), and 600 nm (red spectrum) monitoring the excited state deactivation.

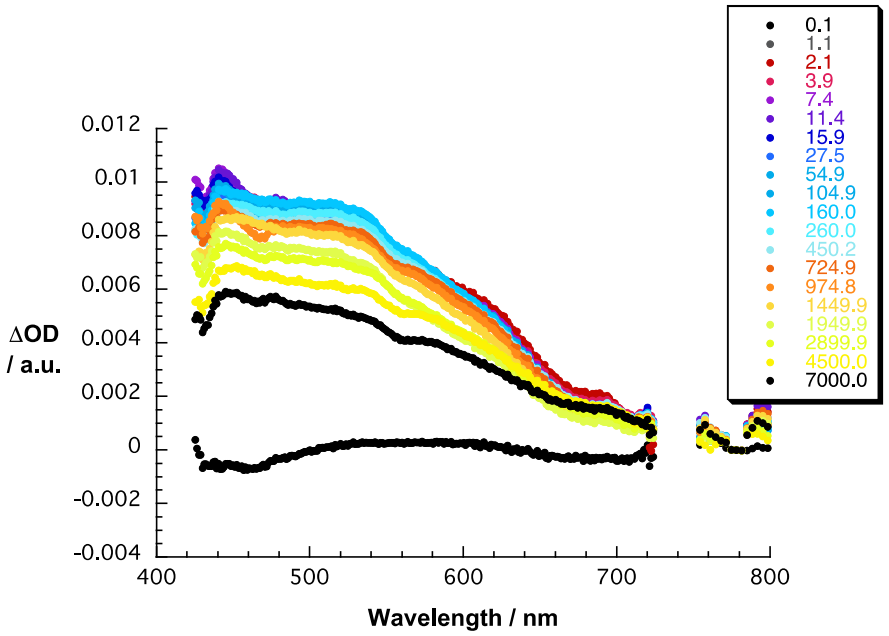


**Figure S5**: Differential absorption spectra (visible) obtained upon femtosecond pump probe experiments (387 nm) of hemifullerene $C_{30}H_{12}$ in toluene with time delays between 0.1 and 7000.0 ps at room temperature.